Environmental Science and Pollution Research (2023) 30:29392–29406
https://doi.org/10.1007/s11356-022-24318-5

RESEARCH ARTICLE

Solidification/stabilization of chromite ore processing residue via co-sintering with hazardous waste incineration residue

Pengpeng Zhang[1,2] · Linghao Zeng[1,2] · Shihao Zhang[3] · Chuanwei Li[1,2] · Dongwei Li[1,2]

Received: 18 July 2022 / Accepted: 15 November 2022 / Published online: 22 November 2022

Abstract

In order to realize the harmless and resource disposal of hazardous waste incineration residue (HWIR) and chromite ore processing residue (COPR), this paper prepares glass–ceramics by HWIR. The COPR was co-sintered with the base glass of HWIR to realize the solidification and stabilization of COPR. The results shown that the single-stage sintering method has a simple process and low energy consumption, while the two-stage sintering method has better mechanical properties. Chromium in COPR may be solidified/stabilized by physical encapsulation and chemical fixation. When the content of COPR reaches 50%, the leaching concentration of Cr and Cr(VI) in the solidified body of HWIR solidified COPR (IRSC) is less than 5 mg/L, which satisfies the US EPA and CN GB5085.3 standard limits. This study achieves waste control by waste and prepares solidified bodies (IRSC) with good mechanical properties, chemical corrosion resistance, and low leaching concentration of heavy metals, which provides feasibility for its engineering application.

Keywords Chromite ore processing residue · Hazardous waste incineration residue · Glass–ceramics · Sintering · Solidification/stabilization

Introduction

Chromite ore processing residue (COPR) is a toxic and hazardous waste slag created during the manufacture of chromium salt that belongs to HW21 (chromium-containing waste category) in the China National Hazardous Wastes List. COPR contains Cr(VI), which is a teratogen, carcinogen, and mutagen (Li et al. 2017; Xia et al. 2020). Unreasonable storage or disposal will pollute the land, surface water, and groundwater, posing a significant hazard to human life and health (Li et al. 2019; Liu et al. 2018). Thus, reasonable, efficient, and safe disposal of COPR is imperative.

Incineration has experienced significant development in recent years due to its advantages in waste reduction and energy recovery as one of the most frequent techniques of municipal waste management (Krausova et al. 2016; Lach et al. 2018). Hazardous waste incineration residue (HWIR) is a kind of industrial waste generated in the process of waste disposal by incineration. Despite the many benefits of incineration, the HWIR still contains a large number of heavy metals with high migration capacity, such as Cu, Zn, Cr, and others, which may leach out under the action of natural phenomena like acid rain and create serious pollution to the environment (Chiang et al. 2009; Li et al. 2018). Therefore, HWIR is considered hazardous waste, classified as HW18 on China National Hazardous Waste List (Chen et al. 2021). As a result, the safe stabilization of HWIR prior to disposal in landfills or resource use is a pressing issue and crucial in HWIR disposal systems. The common disposal method of HWIR is solidification/stabilization. Due to its excellent mechanical properties and wide range of applications, glass–ceramics has become a hot research issue. Chen et al. (2021) prepared SiO_2-Al_2O_3-Fe_2O_3-CaO glass–ceramics using HWIR. The results showed that the zinc, copper, and

Responsible Editor: Guilherme L. Dotto

Pengpeng Zhang, Linghao Zeng, Shihao Zhang and Chuanwei Li contributed equally to the work.

✉ Dongwei Li
litonwei@cqu.edu.cn

[1] College of Resource and Safety Engineering, Chongqing University, Chongqing 400044, China

[2] State Key Laboratory of Coal Mine Disaster Dynamics and Control, Chongqing University, Chongqing 400044, China

[3] School of Architecture and Urban Planning, Chongqing University, Chongqing 400044, China

chromium present in HWIR glass–ceramic were effectively stabilized by the melting-sintering process.

In recent years, scholars and researchers have developed and perfected many effective technological methods for COPR disposal, mainly including chemical reduction technology (Wang et al. 2017; Zhang et al. 2016), microbial detoxification technology (Lai et al. 2016), resource utilization (Wu et al. 2015), and solidification/stabilization (S/S) (Huang et al. 2016, 2017; Xia et al. 2020). Among them, the S/S technology is one of the most effective and widely used technologies (Malviya and Chaudhary 2006). The S/S technique is highly recommended by the US EPA because of its excellent efficiency and effectiveness in treating solid waste containing heavy metals (Huang et al. 2016; S. Zhao et al. 2019a, b). The S/S method is used to immobilize hazardous pollutants in hazardous wastes by physical or chemical means or to reduce or eliminate their toxic effects by reducing/mitigating their migration and diffusion in the environment (Guo et al. 2017). Glass–ceramics solidification/stabilization, as one of the S/S methods, has the following advantages: hazardous solid waste after high-temperature melting treatment has obvious volume and weight reduction effect; heavy metals in the hazardous waste can be stabilized in disordered glass network structure or lattice structure; the product is highly stable and can be used as secondary resources for road base materials, building decoration materials, and so on (Bernardo et al. 2009; Chu et al. 2013; Zhang et al. 2015a). Consequently, glass–ceramics solidification/stabilization technology is gradually considered as one of the most promising techniques for hazardous waste treatment by virtue of its product safety and technological advancement. Therefore, combining the strengths of common disposal methods of HWIR and COPR, this paper will use glass–ceramics solidification/stabilization to achieve the environmentally sound disposal.

Glass–ceramics is a polycrystalline composite material with uniform distribution of glass and microcrystalline phases made by controlled crystallization of a base glass with a specific composition during heat treatment, which combines the advantages of both glass and ceramics with good mechanical and physical properties (Chen et al. 2021; Deng et al. 2020; Lin et al. 2021). Glass–ceramics can be made from discarded glass (Monich et al. 2019) or a range of industrial solid wastes, including slag (Ding et al. 2015; Xu et al. 2021), coal gangue (Dang and He 2020; Wei and He 2019), iron tailings (Xu and Zhao 2019; Yao et al. 2016, 2015), and coal fly ash (Zeng et al. 2019; Zhang et al. 2007, 2015a), which include components like silicon, calcium, aluminum, magnesium, and iron, which are necessary for the production of glass–ceramics. Furthermore, glass–ceramics have been employed by certain researchers to solidify heavy metals. Some scholars have already produced solid waste into high value-added glass–ceramic. OuYang et al. (2019) employed a CaO-MgO-Al_2O_3-SiO_2-based glass–ceramics to solidify Cr-containing stainless steel slag effectively. Liu et al. (2020) investigated the solidification mechanism of heavy metals (Cu and Pb) in oil shale ash based glass–ceramics. They found that the Cu was mainly immobilized in the glass–ceramics by forming CuO crystals, while the Pb was effectively solidified mainly in the form of ions uniformly distributed in the amorphous glassy matrix. They also confirmed the double barrier effect of crystals and glassy matrix on heavy metals in glass–ceramics. Furthermore, the HWIR contains the basic components (silicon, calcium, aluminum, magnesium, and iron) for the preparation of glass–ceramics, which is theoretically feasible. However, there is little research on HWIR, and there are few reports on the solidification of heavy metals by HWIR as a curing agent, which is critical for its development and industrial application.

This paper employed only hazardous waste (HWIR) as a raw material to produce glass–ceramics, and chromium in COPR was solidified/stabilized. The impacts of various heat treatment techniques on the characteristics of HWIR-based glass–ceramics (IRGC) were studied by single-factor experiments. Based on the sintering activity and crystallization ability of the base glass of HWIR, the compressive strength, bulk density, acid and alkali corrosion resistance, heavy metal leaching behavior, XRD, FTIR, and SEM of the solidified body of HWIR solidified COPR (IRSC) under varied COPR content were investigated, and the mechanism of co-sintering of HWIR and COPR to solidify Cr is expounded.

Materials and methods

Materials

HWIR comes from Tianzhi Environmental Protection Co., Ltd., located in Chongqing, China. COPR is produced by Chongqing Minfeng Chemical Co., Ltd. in Chongqing, China. The chemical components of HWIR and COPR determined by XRF are shown in Table 1. The main components of HWIR are SiO_2, Cao, Fe_2O_3, and Al_2O_3, which is feasible to prepare SiO_2-Al_2O_3-Fe_2O_3-CaO glass–ceramics. Fe_2O_3, Al_2O_3, Cr_2O_3, and MgO are the primary components of COPR, in which MgO can be used as flux and Fe_2O_3 and Cr_2O_3 can be used as nucleating agents. Moreover, the acid (sulfuric acid, nitric acid, and acetic acid) utilized in this study is analytically pure, and the water used is deionized.

Sample preparation

The HWIR was dried, crushed, filtered (200 mesh), put into corundum crucibles, and heated in a muff furnace from environmental temperature to 1450 °C at a speed of 10 °C/min

Table 1 Chemical components of HWIR and COPR (wt%)

Raw materials	Composition	SiO_2	Fe_2O_3	Al_2O_3	CaO	TiO_2	Na_2O
HWIR		45.09	12.83	11.27	7.60	7.43	4.71
COPR		2.60	41.91	26.10	-	1.31	3.39
Raw materials	Composition	P_2O_5	ZnO	MgO	K_2O	Cr_2O_3	Other
HWIR		3.12	2.34	1.98	1.35	-	2.28
COPR		-	-	10.16	3.39	13.35	1.67

Others (the sum of the oxides with less than 0.5%)

and maintained for 1 h to guarantee the complete molten. The molten liquid was quenched with water to obtain base glass, then dried, crushed, and filtered (200 mesh) for standby. Put 3 g of sieved base glass into a cylindrical corundum crucible mold (20 mm in diameter and height). Gently shake the mold to minimize gaps, and assure a flat surface. Then, the mold was put into the muff furnace and heated to prepare IRGC using single-stage heat treatment and two-stage heat treatment regime (Table 2). The single-stage heat treatment system refers to heating the sample from room temperature to sintering temperature in a muffle furnace and then maintaining it for a certain time (Table 2: sintering time). The two-stage heat treatment system refers to that the sample is heated from room temperature to nucleation temperature in a muffle furnace for a certain time (nucleation time) and then heated to crystallization temperature for a certain time (nucleation time). The heating rate in the heat treatment regime is 8 °C/min.

A certain proportion (10 ~ 50%) of COPR is used to replace the base glass of the HWIR. The other procedure is identical to the preparation of the HWIR based glass–ceramic. The sample is heated to the corresponding temperature at 8 ℃/min and cooled in the furnace to obtain the IRSC.

Performance test of glass–ceramics and solidified body

Physical performance test

The physical properties of the manufactured samples include compressive strength test and bulk density test. The compressive strength is determined by using universal testing equipment (AGN-250, Shimadzu, Japan) to test the average value of three parallel samples.

Corrosion resistance test

The corrosion resistance test is conducted with reference fine ceramics-determination of corrosion resistance of monolithic ceramics in acid and alkaline solutions (CN JC/T2138-2012). The corrosion solutions are 3.0 mol/L sulfuric acid and 6.0 mol/L sodium hydroxide solutions, respectively. After washing with deionized water and drying, the mass of

Table 2 Experimental design of heat treatment method

ID	Heat treatment method	Nucleation temperature	Nucleation time	Crystallization temperature	Crystallization time
NT1	Two-stage heat treatment regime	690 ℃	1 h	1080	1 h
NT2		720 ℃			
NT3		750 ℃			
NT4		780 ℃			
NT5		810 ℃			
CT1		780 ℃	1 h	950 ℃	1 h
CT2				1000 ℃	
CT3				1080 ℃	
CT4				1150 ℃	
ID	Heat treatment method	Sintering temperature	Sintering time		
ST1	Single-stage heat treatment regime	850 ℃	1 h		
ST2		950 ℃			
ST3		1050 ℃			
ST4		1080 ℃			
ST5		1150 ℃			

the corroded sample was weighed to calculate the weight loss percentage.

Total concentration and leaching concentration test

(1) The determination of total chromium in HWIR and COPR shall be carried out according to the determination of total chromium in solid waste flame atomic absorption spectrophotometry (CN HJ 749–2015). The total content of hexavalent chromium in HWIR and COPR is determined by solid waste-determination of hexavalent chromium by alkaline digestion/flame atomic absorption spectrophotometric (CN HJ 687–2014).

(2) The sulfuric acid and nitric acid method (CN HJ/T 299–2007) and toxicity characteristic leaching procedure (TCLP) method were used to investigate the leaching behavior of chromium (including total chromium and hexavalent chromium) in raw materials (HWIR and COPR) and solidified body (IRSC). The extractant solution of sulfuric acid and nitric acid method is to mix sulfuric acid and nitric acid with a mass ratio of 2:1 and drop them into deionized water to generate a solution with a pH of 3.20 ± 0.05; the solid–liquid ratio is 10:1. Regarding the TCLP method, the extractant solution was prepared by adjusting the pH of the solution at 2.88 ± 0.05 with the help of acetic acid; the solid–liquid ratio is 20:1. After the leaching solution was filtered, the concentration of total chromium was determined by the flame atomic method, and the concentration of hexavalent chromium was determined according to the solid waste determination of chromium (VI)-diphenylcarbohydrazide spectrometric method (CN GB/T 1555.4–1995). The solidification efficiency was evaluated using the following formula:

$$\text{Solidification efficiencies} = 1 - \frac{\text{Quality of each toxic heavy metal in the leaching solution}}{\text{Total mass of each toxic heavy metal in the initial solid}}$$

Characteristic analysis of glass–ceramics and solidified body

The X-ray fluorescence (XRF, Shimadzu, PerkinElmer) was employed to analyze the chemical composition of the HWIR and COPR. The thermal behavior of the HWIR base glass was investigated by differential scanning calorimetry (DSC, STA44PF3, NETZSCH) with a heating rate of 20 °C/min from ambient temperature to 1200 °C. The crystal phase analysis of the raw materials, IRGC and IRSC, was carried out by X-ray diffraction (XRD, PANalytical B·V., the Netherlands) under the conditions of 40 kV and 30 mA CuKα radiation, and the 2θ degree scan range was from 5° to 85°. The Fourier transform figure groups contained in the raw material, IRGC and IRSC in the range of 400~2000 cm^{-1}. The microstructures of the glass–ceramic samples were observed by field emission scanning electron microscopy (FE-SEM, JEOL JSM-7800F, Japan).

Result and discussion

DSC curve and heat treatment temperature design

The results of DSC and thermogravimetric analysis of the HWIR base glass are shown in Fig. 1. The thermogravimetric results show almost no mass loss in the tested range. The DSC curve shows that the glass transition temperature (Tg) of the HWIR base glass occurs around 661 °C and the crystallization process takes place between 870 and 1170 °C, and a peak temperature (Tp) of 1080 °C. The exothermic peak of HWIR base glass has a wide shape and a large span (300 °C), which is consistent with the powder sintering mechanism (Chen et al. 2021). Studies have shown that the nucleation temperature is frequently 50 ~ 100 ℃ higher than the glass transition temperature (Wang et al. 2013; Yalamaç et al. 2020). According to the DSC curve, the initial crystallization temperature is 870 ℃, which is near to the nucleation temperature. Therefore, two heat treatment methods (single-stage and two-stage) are selected for further experiments (Table 2). According to the data of DSC curve, the single-stage heat treatment selects the sintering temperature around the exothermic crystallization peak, i.e., 850 ℃, 950 ℃, 1050 ℃, 1080 ℃, and 1150 ℃. The nucleation temperature in the two-step process is 690 ℃, 720 ℃, 750 ℃, 780 ℃, and 810 ℃ according to the nucleation temperature 50 ~ 100 ℃ higher than the Tg. The crystallization temperature is within the crystallization exothermic peak, which is 920 ℃, 1000 ℃, 1080 ℃, and 1150 ℃. The heating rate is set at 8 ℃/min, and the holding period is set at 1 h based on our previous research (Chen et al. 2021).

Optimization of the heat treatment regime for the preparation of IRGC

Influence of two-stage heat treatment regime on the performance of IRGC

Figure 2 a and b show the effect of nucleation temperature and crystallization temperature with respect to the compressive strength and bulk density of IRGC. The nucleation temperature has a strong influence on the nucleation process of glass–ceramics. According to Fig. 2a, the glass–ceramic sample obtained the maximum compressive strength

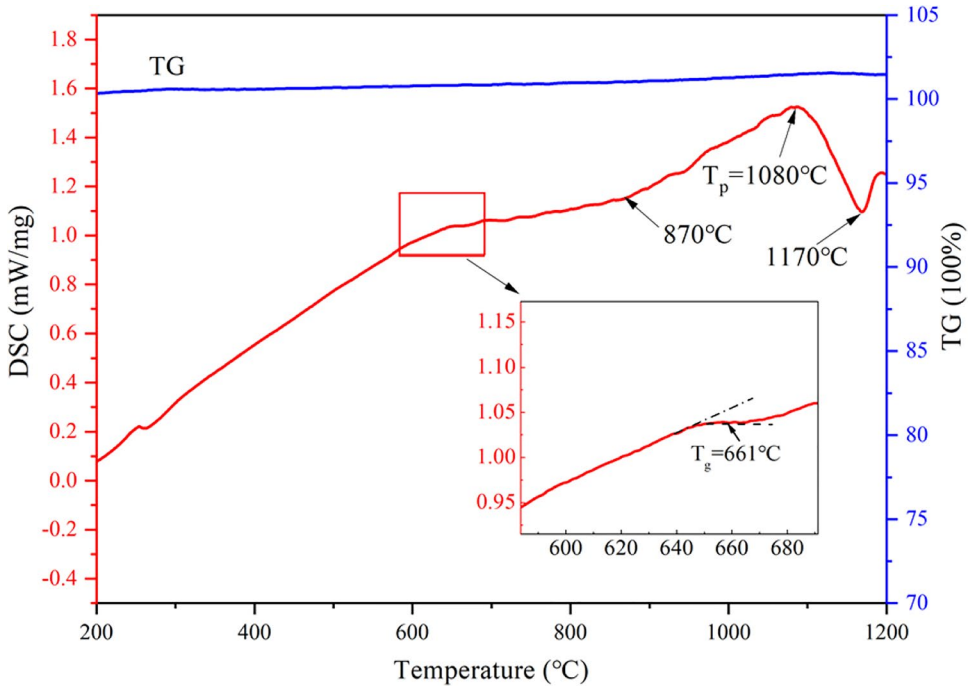

Fig. 1 TG-DSC curve of the HWIR base glass

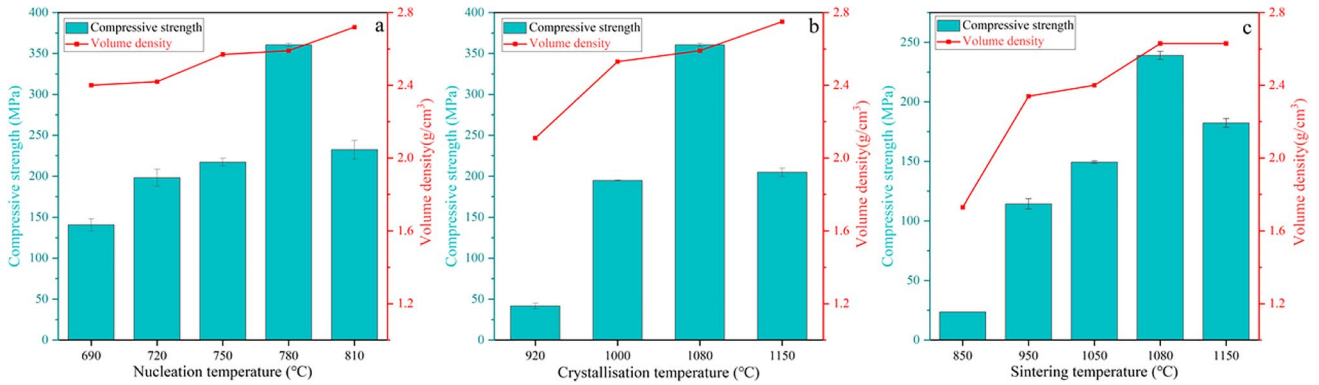

Fig. 2 Effect of heat treatment system on the compressive strength and volume density of IRGC (**a** nucleation temperature, **b** crystallization temperature, **c** single-stage sintering temperature)

(359.04 MPa) at the nucleation temperature of 780 ℃. The increase and decrease of nucleation temperature resulted in the decrease of compressive strength. This is because an incorrect nucleation temperature during the sintering process will prevent the production of crystal nuclei in the sample. The reduction of nucleation leads to a lower crystallinity of the sample, which negatively affects the glass–ceramic properties (Yalamaç et al. 2020). The bulk density of glass–ceramics rises as the nucleation temperature rises. As the temperature of nucleation increases, the sintering between glass particles is promoted, and the increase of the number of crystal nuclei provides the foundation for further crystals development, resulting in tighter crystal structure and increased compressive strength and density. An akin phenomenon was also discovered by Zhang et al. (2015b). Considering the compressive strength, density and energy consumption, 780 ℃ is selected as the nucleation temperature for follow-up investigation.

The crystallization temperature mainly has a strong influence on the crystallization process of glass–ceramics. Figure 2b illustrates that the IRGC compressive strength first grows and then decreases with the increase of crystallization temperature, with 1080 °C serving as the tipping point. The strength of glass–ceramics can be impacted by multiple parameters, counting densification degree, glassy and crystalline phases content, and crystal internal structure (Bernardo et al. 2009; Cheng et al. 2011). The precipitation and growth of crystals are increased as the crystallization

temperature rises, and the crystal phase and glass phase bite each other to form a network crystal structure, increasing the compressive strength of IRGC. This could be attributed to a rise in crystallization temperature at the suitable nucleation temperature, resulting in the rapid sample shrinkage and density increase (Chen et al. 2021; Zhang et al. 2015b). Continuing to increase the temperature will cause the sample's crystals to grow out of control, possibly melting the crystal grains. Considering the compressive strength, bulk density, and energy consumption, 1080 °C can be considered the optimal crystallization temperature.

Influence of single-stage heat treatment regime on the performance of IRGC

Figure 2C demonstrates the influence of single-stage sintering temperature on the compressive strength and bulk density of IRGC. As the sintering temperature increases, the compressive strength increased first and then decreased, reaching the maximum value (239.02 MPa) at 1080 ℃, while the density of samples increased with the increase of sintering temperature, reaching the maximum value (2.63 g/cm^3) at 1080 ℃ and 1150 ℃. The lower sintering temperature will restrict particle migration, increase the difficulty of particle rearrangement during the sintering process and result in low sintering densification (Zhang et al. 2015b). Hence, the compressive strength and density of the sample are low at 850 ~ 1050 ℃. When the sintering temperature is suitable for glass crystallization, the glass particles show liquid viscous flow mass transfer driven by their surface energy. The acceleration of mass transfer speed promotes particle migration and rearrangement, and the sintering between glass particles is more compact. The number of crystals in the sintered body is growing, and the crystal structure is becoming more compact, showing higher compressive strength and density (Cheng et al. 2011; Zhang et al. 2015b). However, excessively high sintering temperature will cause excessive crystal growth and even grain melting, which may lead to structural defects and a decrease of compressive strength (Karayannis et al. 2017; Yalamaç et al. 2020).

Comparing the mechanical properties of the glass–ceramics prepared by the two heat treatment methods, it can be seen that the physical properties of the IRGC obtained by the two-stage heat treatment are better than those obtained by the single-stage heat treatment. The sintering time in the single-stage heat treatment system is 1 h, and the sintering time in the two-stage heat treatment system is 2 h (nucleation time 1 h and crystallization temperature 1 h). Obviously, the single-stage method has lower energy consumption. The single-stage heat treatment method still offers good performance with a simple process and lower energy consumption. The two methods have their advantages, and the subsequent solidification experiments of COPR are carried out using the heat treatment system obtained above.

Solidification/stabilization of chromium residues

Compressive strength and volume density of IRSC

According to the experimental results in Chapter 3.2, the sintering temperature of the single-stage heat treatment is 1080 ℃, the nucleation temperature of the two-stage heat treatment is 780 ℃, and the crystallization temperature is 1080 ℃. According to the above heat treatment system, using the activity of the HWIR base glass, the COPR is partially replaced (10 ~ 50%) of the HWIR base glass by sintering to prepare IRSC to achieve the S/S of the COPR. Figure 3 shows the effect of the percentage of COPR content on the compressive strength and volume density of IRSC. The compressive strength gradually decreased with the content of COPR, while the volume density trends to grow first and then decrease. The higher the content of COPR, the more obvious the reduction in compressive strength. Due to COPR containing low Ca and Si content and being dominated by crystalline phases, it is not conducive to the crystallization process of glass–ceramics, resulting in a decrease in compressive strength. However, Fe_2O_3 and Cr_2O_3 in COPR and TiO_2 in HWIR form composite nucleating agents, which reduce the Tg and Tp and promote the further precipitation of crystals (Alizadeh et al. 2007; Zhang et al. 2018b). Thus, the decline of compressive strength is delayed to a certain extent. In addition, the compressive strength of IRSC created by the two-stage heat treatment is higher than that by the single-stage, which is consistent with the experimental results in Chapter 3.2. Suitable nucleation temperature and nucleation time promote the increase of the number of crystal nuclei, which lays the foundation for the subsequent crystallization process (Cheng et al. 2011). Nonetheless, the compressive strength of the solidified body reaches 11.20 MPa (single-stage) and 12.46 MPa (two-stage) when COPR is mixed at 50%, which meets the strength demands for building materials (> 10 MPa) and landfills (> 0.34 MPa) (Huang et al. 2016, 2017; Pandey et al. 2012). As for the density, the composite crystal nucleating agent promotes the densification and shrinkage between the glass particles to a degree, resulting in a partial increase in density of 10%. However, the density decreases dramatically with the increase of COPR content. This is because the substances contained in COPR are stable crystalline substances with low surface energy, which inhibit the particle migration and rearrangement of amorphous base glass in the densification process, resulting in the reduction of density. An akin phenomenon was also discovered by Zhang et al. (2015b).

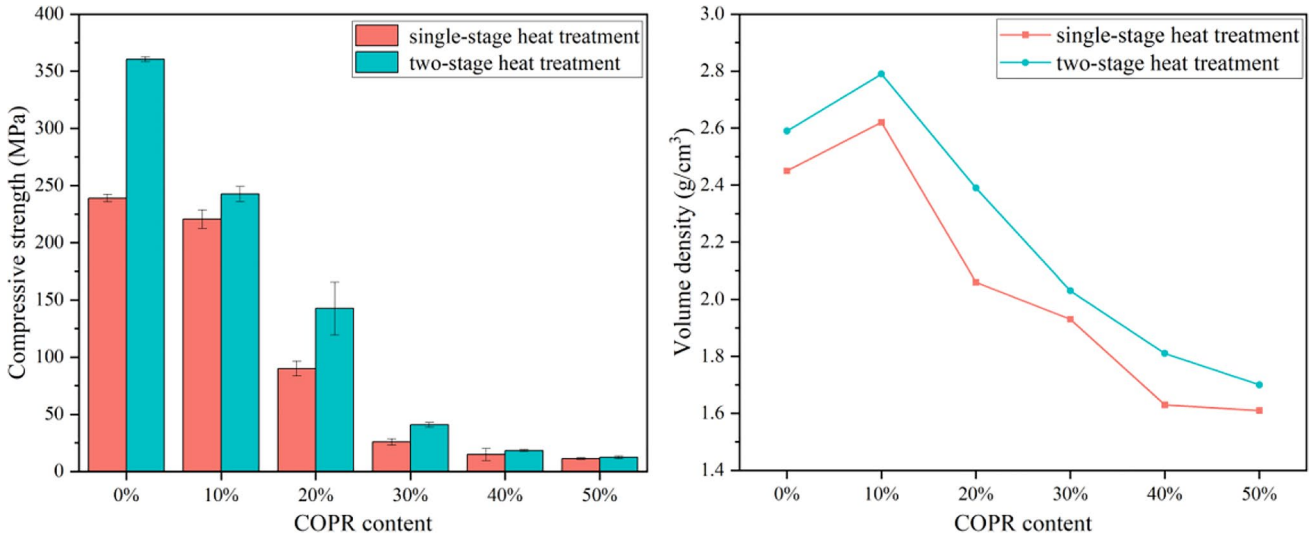

Fig. 3 Compressive strength and volume density of IRSC with different COPR content

Corrosion resistance test of IRSC

The IRSC was tested for acid and alkali corrosion resistance according to Sect. 3.2. The mass loss rate of acid and alkali corrosion resistance of IRSC is shown in Fig. 4. The mass loss rate of IRSC showed an upward trend with the increase of COPR content. At a low COPR level, the combination of glass and microcrystalline phases provides a dense and low porosity structure that inhibits external assault ions from entering. The mass loss rate of alkali corrosion resistance is 0.56% (single stage) and 0.53% (two stage) at 50% COPR, and the alkali resistant mass loss rate is less than 0.5% with other proportions. When the mixing ratio is 30%, the mass loss rate of acid corrosion resistance is 0.41 (single stage) and 0.35 (two stage). The mass loss rate of acid corrosion resistance is significantly higher than alkali corrosion resistance (Liao et al. 2017). IRSC samples with 40% and 50% COPR showed obvious corrosion on the surface, and the stability of the samples deteriorated. The presence of excessive COPR causes a loss of overall strength. This is because the alkali metal cations in the glass phase have better mobility and binding than the ions in the crystalline phase, as well as increased reaction capabilities when meeting corrosive solution. Therefore, the initial chemical corrosion usually occurs in the glass phase, which involves the ion exchange reaction between hydrogen ions and alkali metal cations in the glass phase, followed by tetrahedral structures in silicate or aluminosilicate which may be eroded by the hydration process, so as to weaken its chemical corrosion resistance and show

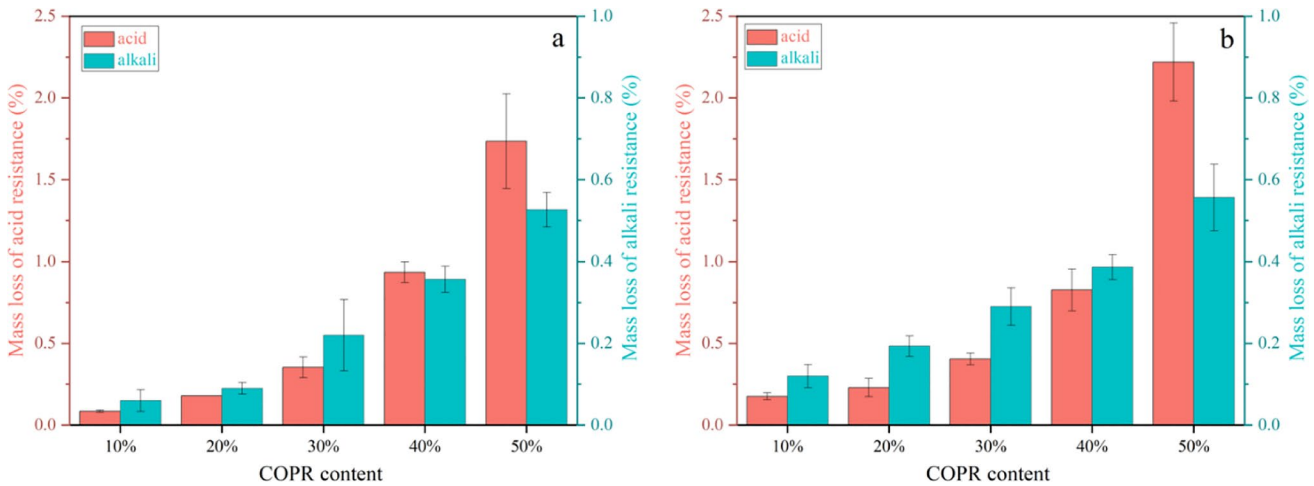

Fig. 4 The mass loss rate of acid and alkali corrosion resistance of IRSC (**a** two-stage heat treatment, **b** single-stage heat treatment)

a faster weight loss rate (Yongsheng et al. 2020; Zhang et al. 2018a), while the alkaline environment will form a soluble calcium silicate and magnesium silicate protective film on the corrosion surface of the sample, which hinders the further corrosion of the alkaline solution (Zhang et al. 2019a). When the proportion of COPR is less than or equal to 30%, the IRSC samples still have good chemical corrosion resistance (mass loss rate less than 0.5%) even in extremely acidic and alkaline environments.

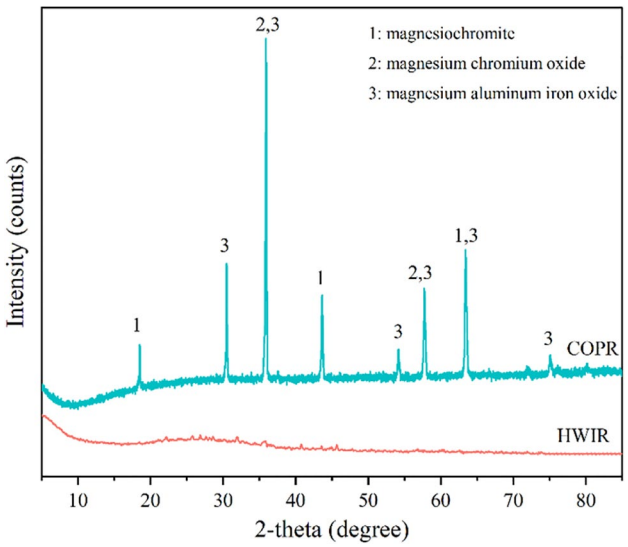

Fig. 5 The XRD patterns of HWIR and COPR

XRD analysis

Figure 5 shows the XRD patterns of HWIR and COPR. The XRD spectrum of HWIR illustrates a broad steamed bread peak in the range of 20°~40°, which suggests that HWIR is composed mainly of amorphous material (Huang et al. 2016). In contrast, COPR is highly crystalline and contains a variety of crystalline phases, mainly containing magnesiochromite (PDF# 87–1175), magnesium chromium oxide (PDF# 77–0007), and magnesium aluminum iron oxide (PDF# 71–1235).

The crystal phase analysis of IRGC and IRSC under different heat treatment conditions was carried out using jade 6.5, and the results are shown in Fig. 6. Comparing the results of the two heat treatment systems, it can be seen that the heat treatment system has little effect on the crystal types precipitated from IRSC, which are pseudobrookite (Fe_2TiO_5) (PDF# 470–2728), hematite (Fe_2O_3) (PDF# 85–0987), anorthite ($CaAl_2Si_2O_8$) (PDF# 76–0948), and diiron silicate (Fe_2SiO_4) (PDF# 80–1625); there are only slight differences in the diffraction peak intensities of different crystals. The HWIR and COPR contain high Fe_2O_3 content. In the sintering process, Fe_2O_3 and TiO_2 react to form pseudobrookite crystals. The main crystalline phase of IRGC is anorthite (PDF# 76–0948), and the diffraction peak intensity of the anorthite crystal in the two-stage heat treatment is significantly higher than that in the single-stage heat treatment, which also explains that the compressive strength of the two-stage process is obviously higher than that of the single-stage process. This is because the two-stage heat treatment has appropriate nucleation time, which provides a basis for the subsequent precipitation of anorthite crystal.

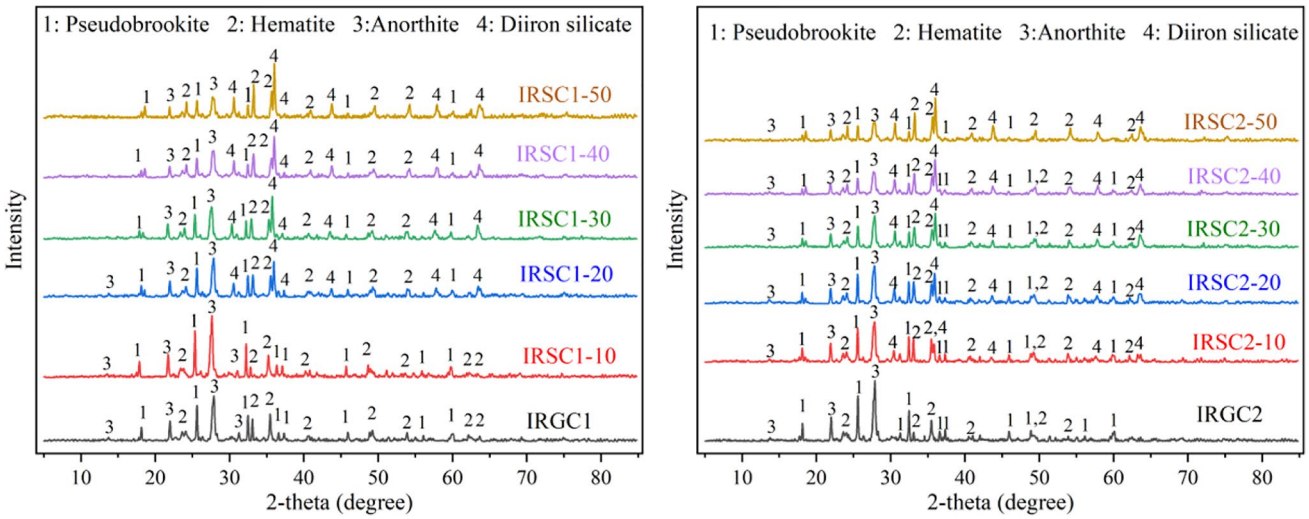

Fig. 6 The XRD patterns of IRGC and IRSC (IRGC1, single-stage heat treatment of IRGC; IRGC2, two-stage heat treatment of IRGC; IRSC1-10, single-stage heat treatment of IRGC with 10% COPR)

With the increase of COPR, the diffraction peak intensities of pseudobrookite and anorthite crystalline phases showed a downward trend as a whole, while the diffraction peak intensities of hematite and diiron silicate crystalline phases showed an overall upward trend. When the content of chromium slag is 10%, the diffraction peak intensity of anorthite crystal in the single-stage heat treatment is higher than that in the two-stage heat treatment; and a new crystalline phase diiron silicate (PDF# 80–1625) appears in the two-stage IRSC. This may be due to the short nucleation time in the single-stage sintering process. However, the nucleating agents Cr_2O_3 and Fe_2O_3 in the COPR and TiO_2 in the HWIR form a composite nucleating agent, which promotes the crystallization process of anorthite crystal (Zhang et al. 2019a; Zhao et al. 2021). There is little difference of ionic radius between Cr^{3+} (0.063 nm) and Fe^{3+} (0.064 nm). Thus, Cr^{3+} could replace the Fe^{3+} sites in the iron-rich crystalline phase (pseudobrookite) to form sosoloid, thereby realizing the solidification/stabilization of Cr. With the increase of COPR, the main crystal phase of the IRSC changes from anorthite to diiron silica. The increase of COPR leads to the increase of iron and chromium content. The addition of Cr_2O_3 reduces the connection degree of [SiO_4] and [AlO_4] networks and facilitates the formation of more simple silica and alumina groups (Zhang et al. 2020c). It promotes the reduction of anorthite crystals and the increase of diiron silicate.

FTIR analysis

Figure 7 shows the FTIR spectra of IRGC and IRCS with different ratios of COPR. Comparing the analysis of the IRGC1 (single stage) and IRGC2 (two stage) spectra, the overall trend of the absorption peaks of both is basically the same, which corresponds to the same crystalline phase in XRD. The peak at 1622 cm^{-1}–1638 cm^{-1} is owing to the vibration of O–H bond or the bending of the surface O–H group (Mukherjee and Das 2013; Sharma et al. 2013). The strong absorption peaks at 1120 cm^{-1}, 1012 cm^{-1}, 1093 cm^{-1}, and 1027 cm^{-1} are attributed to the asymmetric stretching vibration of Si–O-Si (Al) (Liu et al. 2014; Mao et al. 2016). This suggests that IRGC may have tetrahedral structures of [SiO_4] and [AlO_4]. Also, 687 cm^{-1} and 685 cm^{-1} correspond to symmetric stretching vibrations of Si–O-Al (Luo et al. 2020; Zhao et al. 2019a, b), which contrast with the presence of anorthite crystals in XRD. FTIR band at 624 cm^{-1} can be assigned to Fe–O stretching vibrations (Zayed et al. 2016). The absorption peaks at 575 cm^{-1} and 574 cm^{-1} are attributed to the bond vibration of Fe^{3+}-O in [FeO_4], suggesting that [FeO_4] might be present in the glass network framework (Dantas et al. 2011). The absorption peak at 541 cm^{-1} could be attributed to the vibration of Fe–O (Navarro et al. 2010; Zayed et al. 2016), which is consistent with the XRD pattern of IRGC for hematite and pseudobrookite. And 473 cm^{-1} and 471 cm^{-1} may be due to the presence of Si–O-T (Si, Al, Fe) (M. Zhao et al. 2019a, b). The absorption peaks at 416 cm^{-1} and 428 cm^{-1} are attributed to the bending vibrations of Si–O-Si and O-Si–O (Luo et al. 2020; Xia et al. 2020). With the increase of chromium slag content, the strong absorption peak of IRSC is still between 800 cm^{-1} and 1200 cm^{-1}. Compared with IRGC, there is an obvious trend where the absorption peak shifts to a lower frequency (978 cm^{-1}) from a high frequency (1093 cm^{-1}–1120 cm^{-1}). This phenomenon confirms that the polymerization degree

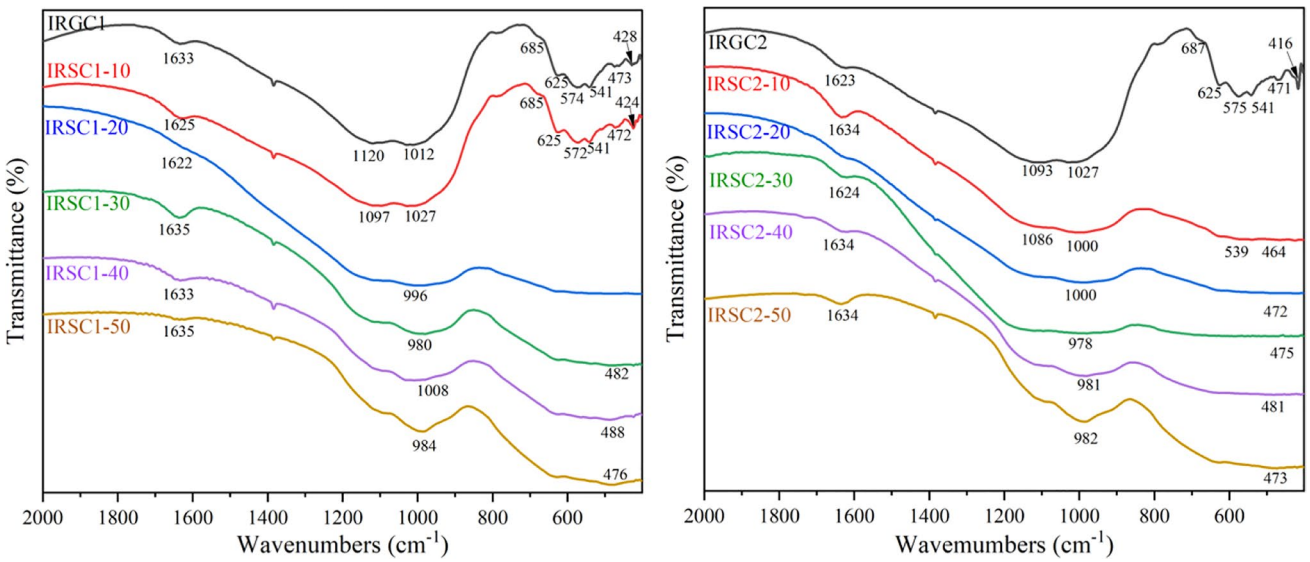

Fig. 7 The FTIR spectra of IRGC and IRCS with different ratios of COPR

of the silicate framework may drop (Dantas et al. 2011). The macroscopic manifestation is a decrease in the mechanical properties of IRCS. The infrared spectrum shows that the structure of IRCS is dominated by [SiO_4], and [AlO_4] and [FeO_4] may be doped into it to form a glass network structure. During the sintering process, Fe^{3+} and Al^{3+} may replace Si^{4+} in [SiO_4], resulting in [AlO_4] and [FeO_4] being negatively charged. Thus, a complicated cationic layer is formed around [AlO_4] and [FeO_4] for charge balancing. At the same time, the Cr^{3+} ion has a small radius and strong polarization and may replace the Ca^{2+} or Na^{+} sites into the network structure (Chen et al. 2021; Huang et al. 2016).

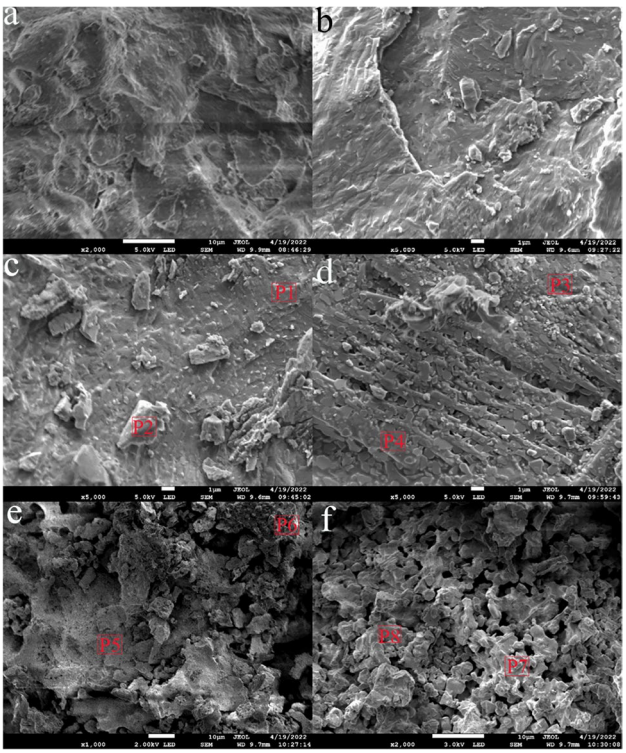

Fig. 8 The SEM micrographs of glass–ceramic samples with different COPR contents

SEM analysis

Figure 8 shows the SEM micrographs of glass–ceramic samples with different COPR contents, in which (a), (c), and (e) are single-stage method and (b), (d), and (f) are two-stage method. Figure 8 a and b show the IRGC prepared by single-stage and two-stage methods. The crystalline and amorphous glassy matrix forms a compact structure without obvious defects on the surface. This phenomenon also indicates the crystallization ability of the incineration residue glass–ceramic samples, which provides support for the good compressive strength of the glass–ceramic samples (Zhang et al. 2020a). Figure 8 c and d shows the COPR doping of 10%. The overall crystallinity of the samples is higher with increasing COPR content, which is also consistent with XRD. This dense and compact microstructure ensures superior compressive strength and physical properties and provides the structural basis for effective curing of heavy metals by physical encapsulation (Zhang et al. 2020b). Figure 8 e and f shows the COPR doping of 40%. The presence of a large number of gaps on the surface of the samples and the lack of formation of a monolith resulted in a decrease in the compressive strength and the curing effect of heavy metals.

In order to further investigate the solidification mechanism of heavy metal, IRSC10 and IRSC40 were selected for energy spectrum scanning, and the specific regions are shown in Fig. 8. According to the energy spectrum data of IRSC in Table 3, the main components of the amorphous glass network in the glass ceramics sample are Si, Al, and O. Combined with the FTIR spectrum, it can be further inferred that there may be some aluminosilicate structure in the glass network of the glass–ceramics sample. The presence of Cr in both the glass and crystal regions of IRSC indicates that the glass–ceramics can effectively solidify the Cr by physical encapsulation (glass network structure wrapping) and chemical fixation (crystal curing). The Cr content in the two-stage method is slightly higher than that in the single-stage method, which is corroborated by the variation of XRD crystals. The solidification effect of glass–ceramics on COPR is limited, so with the increase of COPR content, the content

Table 3 The results of IRSC elemental composition tested by EDS

Sample	Elemental composition (atomic %)						
	O	Al	Si	Ca	Ti	Cr	Fe
P1	66.64	8.26	14.61	3.82	2.61	2.18	1.89
P2	68.21	6.08	12.26	4.66	4.14	2.24	2.41
P3	61.34	5.41	13.93	4.07	7.85	3.15	4.24
P4	66.79	5.13	9.31	2.8	3.58	3.36	9.03
P5	66.04	7.13	17.08	4.06	2.55	1.8	1.33
P6	65.58	3.12	8.61	2.87	8.53	2.95	4.34
P7	64.89	6.65	12.87	3.02	4.55	3.97	4.06
P8	59.84	4.41	7.49	4.15	13.15	4.62	6.35

of Cr and Fe in the sample increases slightly. The solidification effect of glass ceramics on chromium slag is limited, so with the increase of chromium slag content, the content of Cr and Fe in the sample increases slightly. The change of Fe content provides a basis for the formation of diiron silicate in XRD and lays a foundation for the chemical curing of Cr replacement.

Leaching toxicity of raw materials and IRSC

Exploring the total content of heavy metals in raw materials is a crucial index to explore its potential risk. According to the standards in Chapter 2.3.3, the total contents of total chromium and hexavalent chromium in COPR are 40.32 g/kg and 0.61 g/kg, respectively. The chromium in COPR is mainly trivalent chromium (hexavalent chromium accounts for about 1.52%). The heavy metals in HWIR were analyzed by microwave digestion and inductively coupled plasma optical emission spectrometry (ICP-OES). The total content of heavy metals in HWIR is Zn (13.59 g/kg), Cu (2.5 g/kg), Cr (1.8 g/kg), and Pb (0.2 g/kg). Combined with previous studies (Chen et al. 2021), the preparation of glass–ceramics from HWIR under various heat treatment systems has a low leaching concentration of heavy metals, basically less than 1 mg/L. Therefore, the subsequent leaching concentration study in this paper focuses on the effect of COPR, i.e., chromium and hexavalent chromium.

The leaching concentration of raw materials was determined by the sulfuric acid and nitric acid method (S&N) and TCLP methods, as shown in Table 4. The leaching concentrations of total chromium (Cr(T)) in COPR were 58.34 mg/L (S&N) and 31.83 mg/L (TCLP), respectively, exceeding the relevant standards: 15 mg/L (CN GB5085.3–2007) and 5 mg/L (US EPA). The leaching concentrations of Cr(VI) were 45.45 mg/L (S&N) and 26.67 mg/L (TCLP), respectively, exceeding the relevant standards 5 mg/L (CN GB5085.3–2007). The leaching concentration of heavy metals (Zn, Cu) in HWIR did not exceed the relevant limitations, so the subsequent solidification experiments focused on the chromium.

The leaching toxicity of IRSC at different doping ratios (IRSC10-IRSC50) was tested by the S&N method and TCLP method, as shown in Table 4. The leaching concentration of Cr(T) in IRSC is significantly lower than that in COPR. The increase of COPR content leads to the increase of the chromium, resulting in an upward trend of chromium leaching concentration. However, when the COPR was mixed at 50%, the leaching concentrations of Cr(VI) are 1.29 mg/L, 1.64 mg/L, 1.07 mg/L, and 0.94 mg/L, respectively, and the leaching concentrations of Cr(T) are 1.97 mg/L and 1.82 mg/L,2.4 mg/L, and 1.92 mg/L, which are less than the standard limits of Cr(VI) (5 mg/L) and Cr(T) (15 mg/L). It also meets the limit requirement of Cr(VI) (3 mg/L) and Cr(T) (9 mg/L) in China when COPR solidified body enters the general industrial solid waste landfill. The leaching toxicity of IRSC at different doping ratios (IRSC10-IRSC50) was tested by the S&N method and TCLP method, as shown in Table 5. With the increase of the content of COPR, the overall solidification efficiency showed a downward trend. The curing efficiency of total chromium is more than 98%, and that of hexavalent chromium is almost more than 90%, indicating that glass–ceramics could effectively solidify Cr.

Table 4 Leaching concentration of chromium and critical limits

		Sulfuric acid and nitric acid method		TCLP	
		Cr(T) (mg/L)	Cr(VI) (mg/L)	Cr(T) (mg/L)	Cr(VI) (mg/L)
Raw materials	COPR	58.34	45.45	31.83	26.67
	HWIR	0.99	0.73	0.36	0.2
Two-stage heat treatment	IRGC	0.03	0.01	0.05	0.01
	10% COPR	0.02	0.02	0.04	0.01
	20% COPR	0.03	0.02	0.05	0.02
	30% COPR	0.04	0.03	0.21	0.03
	40% COPR	0.72	0.7	0.83	0.04
	50% COPR	1.82	1.64	1.92	0.94
Single-stage heat treatment	IRGC	0.05	0.01	0.05	0.01
	10% COPR	0.04	0.02	0.04	0.01
	20% COPR	0.04	0.02	0.04	0.02
	30% COPR	0.04	0.03	0.2	0.02
	40% COPR	0.76	0.64	0.97	0.1
	50% COPR	1.97	1.29	2.4	1.07
Critical limits		15	5	5	–
		CN GB 5085.3–2007		US EPA	

Table 5 Immobilization efficiencies of chromium from glass–ceramics

		Sulfuric acid and nitric acid method		TCLP	
		Cr(T) (mg/L)	Cr(VI) (mg/L)	Cr(T) (mg/L)	Cr(VI) (mg/L)
Two-stage heat treatment	IRGC	99.89%	93.33%	99.62%	86.67%
	10% COPR	99.96%	90.48%	99.86%	90.48%
	20% COPR	99.97%	95.56%	99.90%	91.11%
	30% COPR	99.97%	97.25%	99.73%	94.50%
	40% COPR	99.62%	87.11%	99.12%	98.53%
	50% COPR	99.24%	88.46%	98.40%	86.77%
Single-stage heat treatment	IRGC	99.77%	96.00%	99.53%	92.00%
	10% COPR	99.92%	94.87%	99.84%	94.87%
	20% COPR	99.96%	98.58%	99.92%	97.16%
	30% COPR	99.97%	98.28%	99.71%	97.70%
	40% COPR	99.57%	88.59%	98.90%	96.43%
	50% COPR	99.22%	91.90%	98.11%	86.57%

Combined with XRD analysis, FTIR analysis, SEM analysis, and leaching concentration of Cr, the decrease of heavy metal (Cr) concentration in COPR may be attributed to two aspects. (1) The heavy metal chromium is probably embedded in the glass network or crystal phase through ionic (Ca^{2+}, Al^{3+}, and Fe^{3+}) exchange to achieve chemical fixation (Chen et al. 2021; Erol et al. 2007; Zhang et al. 2019b). (2) The crystal phase and the glass phase in the IRSC interlock to form a network structure, which gives high strength and allows heavy metals to be encapsulated for physical solidification (Zhang et al. 2020a, b). Combined with compressive strength, bulk density, corrosion resistance, and leaching toxicity, IRCS is a suitable waste-based material with the possibility to prepare building materials.

Conclusions

In this paper, the HWIR is used as the raw material to explore the effect of heat treatment methods (single-stage, two-stage heat treatment system) on the properties of the IRGC, and the COPR is effectively immobilized by using the sintering activity of HWIR base glass. The main conclusions are shown below:

(1) The HWIR rich in SiO_2, Al_2O_3, Fe_2O_3, and CaO facilitates the preparation of SiO_2-Al_2O_3-Fe_2O_3-CaO glass–ceramics. The effects of heat treatment methods on the properties of glass–ceramics were investigated with compressive strength and density as indicators. The two methods have their advantages. The single-stage heat treatment method has a simple process and low energy consumption, while the two-stage heat treatment method has better physical characteristics of IRGC.

(2) With the increase of chromium residue content, the compressive strength, density, and acid and alkali corrosion resistance of IRSC showed a downward trend, and the leaching of Cr(T) and Cr(VI) showed an upward trend. When the proportion of chromium slag is 50%, the compressive strength of IRSC still meets the requirements of compressive strength of building materials (> 10 MPa), and the leaching concentrations of Cr(T) and Cr(VI) are less than 5 mg/L, which meets the leaching standards of US EPA and CN GB5085.3. The XRD, FTIR, and SEM analysis and heavy metal leaching toxicity showed that chromium in COPR was effectively solidified/stabilized in IRSC.

(3) Since the study was conducted under laboratory conditions, the practical application of the project and the cost of the technology were not fully considered. Subsequent studies will focus on how to reduce the cost of the technology and the practical application of the project.

Author contribution Pengpeng Zhang: investigation, formal analysis, writing-original draft. Linghao Zeng: validation, formal analysis. Shihao Zhang: writing-review and editing. Chuanwei Li: resources, validation. Dongwei Li: project administration, supervision.

Funding This study was sponsored by general program of State Key Laboratory of Coal Mine Disaster Dynamics and Control, Chongqing University (No. 2011DA105287-MS202121) and Graduate Research and Innovation Foundation of Chongqing, China (grant number: CYB22025).

Data availability All data generated or analyzed during this study are included in this published article.

Declarations

Ethics approval and consent to participate Not applicable.

Consent for publication Not applicable.

Competing interests The authors declare no competing interests.

References

Alizadeh P, Yousefi M, Yekta BE, Ghafoorian N, Molaie F (2007) Sintering behavior of SiO_2-CaO-MgO (Na_2O) glass–ceramics system. Ceram Int 33:767–771. https://doi.org/10.1016/j.ceramint.2006.01.023

Bernardo E, Scarinci G, Edme E, Michon U, Planty N (2009) Fast-sintered gehlenite glass–ceramics from plasma-vitrified municipal solid waste incinerator fly ashes. J Am Ceram Soc 92:528–530. https://doi.org/10.1111/j.1551-2916.2008.02892.x

Chen H, Lin H, Zhang P, Yu L, Chen L, Huang X, Jiao B, Li D (2021) Immobilisation of heavy metals in hazardous waste incineration residue using SiO2–Al_2O_3–Fe_2O_3–CaO glass-ceramic. Ceram Int 47:8468–8477. https://doi.org/10.1016/j.ceramint.2020.11.213

Cheng TW, Tu CC, Ko MS, Ueng TH (2011) Production of glass–ceramics from incinerator ash using lab-scale and pilot-scale thermal plasma systems. Ceram Int 37:2437–2444. https://doi.org/10.1016/j.ceramint.2011.05.088

Chiang KY, Tsai CC, Wang KS (2009) Comparison of leaching characteristics of heavy metals in APC residue from an MSW incinerator using various extraction methods. Waste Manage 29:277–284. https://doi.org/10.1016/j.wasman.2008.04.006

Chu TC, Wang KS, Lin KL, Chien CC, Chen JH (2013) Synthesis of waste-derived glass-ceramics from MSWI fly ash and EAF dust: kinetics of nucleation and crystallization. Environ Prog Sustain Energy 32:480–488. https://doi.org/10.1002/ep.11647

Dang W, He HY (2020) Glass-ceramics fabricated by efficiently utilizing coal gangue. J Asian Ceram Soc 8:365–372. https://doi.org/10.1080/21870764.2020.1743417

Dantas NO, Ayta WEF, Silva ACA, Cano NF, Silva SW, Morais PC (2011) Effect of Fe_2O_3 concentration on the structure of the SiO_2–Na_2O–Al_2O_3–B_2O_3 glass system. Spectrochim Acta Part A Mol Biomol Spectrosc 81:140–143. https://doi.org/10.1016/j.saa.2011.05.074

Deng L, Jia R, Yun F, Zhang X, Li H, Zhang M, Jia X, Ren D, Li B (2020) Influence of Cr2O3 on the viscosity and crystallization behavior of glass ceramics based on blast furnace slag. Mater Chem Phys 240:122212. https://doi.org/10.1016/j.matchemphys.2019.122212

Ding L, Ning W, Wang Q, Shi D, Luo L (2015) Preparation and characterization of glass–ceramic foams from blast furnace slag and waste glass. Mater Lett 141:327–329. https://doi.org/10.1016/j.matlet.2014.11.122

Erol M, Küçükbayrak S, Ersoy-Meriçboyu A (2007) Production of glass-ceramics obtained from industrial wastes by means of controlled nucleation and crystallization. Chem Eng J 132:335–343. https://doi.org/10.1016/j.cej.2007.01.029

Guo B, Liu B, Yang J, Zhang S (2017) The mechanisms of heavy metal immobilization by cementitious material treatments and thermal treatments: a review. J Environ Manag 193:410–422. https://doi.org/10.1016/j.jenvman.2017.02.026

Huang X, Huang T, Li S, Muhammad F, Xu G, Zhao Z, Yu L, Yan Y, Li D, Jiao B (2016) Immobilization of chromite ore processing residue with alkali-activated blast furnace slag-based geopolymer. Ceram Int 42:9538–9549. https://doi.org/10.1016/j.ceramint.2016.03.033

Huang X, Zhuang R, Muhammad F et al (2017) Solidification/stabilization of chromite ore processing residue using alkali-activated composite cementitious materials. Chemosphere 168:300–308. https://doi.org/10.1016/j.chemosphere.2016.10.067

Karayannis V, Moutsatsou A, Domopoulou A, Katsika E, Drossou C, Baklavaridis A (2017) Fired ceramics 100% from lignite fly ash and waste glass cullet mixtures. J Build Eng 14:1–6. https://doi.org/10.1016/j.jobe.2017.09.006

Krausova K, Gautron L, Karnis A, Catillon G, Borensztajn S (2016) Glass ceramics and mineral materials for the immobilization of lead and cadmium. Ceram Int 42:8779–8788. https://doi.org/10.1016/j.ceramint.2016.02.119

Lach M, Mierzwinski D, Korniejenko K, Mikula J, Hebda M (2018) Geopolymers as a material suitable for immobilization of fly ash from municipal waste incineration plants. J Air Waste Manag Assoc 68:1190–1197

Lai CY, Zhong L, Zhang Y, Chen JX, Wen LL, Shi LD, Sun YP, Ma F, Rittmann BE, Zhou C, Tang Y, Zheng P, Zhao HP (2016) Bioreduction of chromate in a methane-based membrane biofilm reactor. Environ Sci Technol 50:5832–5839. https://doi.org/10.1021/acs.est.5b06177

Li W, Ma Z, Huang Q, Jiang X (2018) Distribution and leaching characteristics of heavy metals in a hazardous waste incinerator. Fuel 233:427–441. https://doi.org/10.1016/j.fuel.2018.06.041

Li Y, Cundy AB, Feng J, Fu H, Wang X, Liu Y (2017) Remediation of hexavalent chromium contamination in chromite ore processing residue by sodium dithionite and sodium phosphate addition and its mechanism. J Environ Manag 192:100–106. https://doi.org/10.1016/j.jenvman.2017.01.031

Li Y, Liang J, Yang Z, Wang H, Liu Y (2019) Reduction and immobilization of hexavalent chromium in chromite ore processing residue using amorphous FeS_2. Sci Total Environ 658:315–323. https://doi.org/10.1016/j.scitotenv.2018.12.042

Liao C-Z, Tang Y, Lee PH, Liu C, Shih K, Li F (2017) Detoxification and immobilization of chromite ore processing residue in spinel-based glass-ceramic. J Hazard Mater 321:449–455. https://doi.org/10.1016/j.jhazmat.2016.09.035

Lin H, Zhang P, Zeng L, Jiao B, Shiau Y, Li D (2021) Preparation of glass-ceramics via cosintering and solidification of hazardous waste incineration residue and chromium-containing sludge. ACS Omega 6:23723–23730. https://doi.org/10.1021/acsomega.1c01659

Liu L, Yu H, Li Y, Zhang Z (2020) Stabilization behavior and mechanism of heavy metals in eco-friendly glass-ceramics derived from wastes. J Clean Prod 269:122417. https://doi.org/10.1016/j.jclepro.2020.122417

Liu M, Zhao L, Liu Y, Lan Z, Chang L, Li Y, Yu H (2014) Role of heavy metal ions in the formation of oxyfluoride glasses and glass ceramics. J Mater Sci Technol 30:1213–1216. https://doi.org/10.1016/j.jmst.2014.02.003

Liu Y, Zhu H, Zhang M, Chen R, Chen X, Zheng X, Jin Y (2018) Cr(VI) recovery from chromite ore processing residual using an enhanced electrokinetic process by bipolar membranes. J Membr Sci 566:190–196. https://doi.org/10.1016/j.memsci.2018.07.079

Luo Z, He F, Zhang W, Xiao Y, Xie J, Sun R, Xie M (2020) Effects of fluoride content on structure and properties of steel slag glass-ceramics. Mater Chem Phys 242:122531. https://doi.org/10.1016/j.matchemphys.2019.122531

Malviya R, Chaudhary R (2006) Factors affecting hazardous waste solidification/stabilization: a review. J Hazard Mater 137:267–276. https://doi.org/10.1016/j.jhazmat.2006.01.065

Mao L, Gao B, Deng N, Liu L, Cui H (2016) Oxidation behavior of Cr(III) during thermal treatment of chromium hydroxide in the presence of alkali and alkaline earth metal chlorides.

Chemosphere 145:1–9. https://doi.org/10.1016/j.chemosphere.2015.11.053

Monich PR, Desideri D, Bernardo E (2019) Low temperature upcycling of vitreous byproduct of the MSW plasma processing into multifunctional porous glass-ceramics. Adv Appl Ceram 118:366–371. https://doi.org/10.1080/17436753.2019.1595265

Mukherjee DP, Das SK (2013) SiO_2–Al_2O_3–CaO glass-ceramics: effects of CaF_2 on crystallization, microstructure and properties. Ceram Int 39:571–578. https://doi.org/10.1016/j.ceramint.2012.06.066

Navarro C, Díaz M, Villa-García MA (2010) Physico-chemical characterization of steel slag. Study of its Behavior under Simulated Environmental Conditions. Environ Sci Technol 44:5383–5388. https://doi.org/10.1021/es100690b

OuYang S, Zhang Y, Chen Y, Zhao Z, Wen M, Li B, Shi Y, Zhang M, Liu S (2019) Preparation of glass-ceramics using chromium-containing stainless steel slag: crystal structure and solidification of heavy metal chromium. Sci Rep 9:1964. https://doi.org/10.1038/s41598-018-37996-4

Pandey B, Kinrade SD, Catalan LJJ (2012) Effects of carbonation on the leachability and compressive strength of cement-solidified and geopolymer-solidified synthetic metal wastes. J Environ Manag 101:59–67. https://doi.org/10.1016/j.jenvman.2012.01.029

Sharma K, Bhattacharya S, Bhushan KG, Deo MN, Kothiyal GP (2013) Structural and surface studies on calcium phospho-silicate glass-ceramics containing zinc and iron oxide. J Non-Cryst Solids 376:221–228. https://doi.org/10.1016/j.jnoncrysol.2013.04.021

Wang J, Cheng J, Deng Z (2013) Effect of alkali metal oxides on viscosity and crystallization of the MgO–Al_2O_3–SiO_2 glasses. Physica B 415:34–37. https://doi.org/10.1016/j.physb.2013.01.039

Wang X, Zhang J, Wang L, Chen J, Hou H, Yang J, Lu X (2017) Long-term stability of $FeSO_4$ and H_2SO_4 treated chromite ore processing residue (COPR): importance of H^+ and SO_4^{2-}. J Hazard Mater 321:720–727. https://doi.org/10.1016/j.jhazmat.2016.09.048

Wei D, He HY (2019) High strength glass-ceramics sintered with coal gangue as a raw material. Sci Sinter 51:285–294

Wu J, Li C, Yang F (2015) The disposition of chromite ore processing residue (COPR) incorporating industrial symbiosis. J Clean Prod 95:156–162. https://doi.org/10.1016/j.jclepro.2015.02.041

Xia M, Muhammad F, Zhao S, Yu L, Lin H, Huang X, Jiao B, Shiau YC, Li D (2020) Detoxification and immobilization of chromite ore processing residue using the alkali-activated cementitious materials mixed with ascorbic acid. J Environ Manag 265:110350. https://doi.org/10.1016/j.jenvman.2020.110350

Xu C, Zhao J (2019) Preparation of iron tailings glass-ceramics by sol-gel method. IOP Conf Ser Mater Sci Eng 544:012002. https://doi.org/10.1088/1757-899X/544/1/012002

Xu W, Shen K, Cao Z, Liu F, Zhang Y, Zhang T, Wu N, Ouyang S (2021) Crystallization and thermal stability effects on tailings glass-ceramics by various heat treating processes. Mater Chem Phys 263:124334. https://doi.org/10.1016/j.matchemphys.2021.124334

Yalamaç E, Sutcu M, Ergani ES (2020) Effect of heat treatment parameters on the crystallization of feldspathic-based dental glass-ceramics. J Asian Ceram Soc 8:685–693. https://doi.org/10.1080/21870764.2020.1774973

Yao R, Liao S, Chen X, Tang G, Wang G, Zheng F (2016) Effects of ZnO and NiO on material properties of microwave absorptive glass-ceramic tile derived from iron ore tailings. Ceram Int 42:8179–8189. https://doi.org/10.1016/j.ceramint.2016.02.025

Yao R, Liao S, Dai C, Liu Y, Chen X, Zheng F (2015) Preparation and characterization of novel glass–ceramic tile with microwave absorption properties from iron ore tailings. J Magn Magn Mater 378:367–375. https://doi.org/10.1016/j.jmmm.2014.11.066

Yongsheng D, Jie M, Yu S, Xuefeng Z, Hongxia Z, Hua C, Shunli O, Li B (2020) Crystallization characteristics and corrosion properties of slag glass-ceramic prepared from blast furnace slag containing rare earth. J Non-Cryst Solids 532:119880. https://doi.org/10.1016/j.jnoncrysol.2019.119880

Zayed MA, Ahmed MA, Imam NG, El Sherbiny DH (2016) Analytical characterization of hematite / magnetite ferrofluid nanocomposites for hyperthermia purposes. J Supercond Nov Magn 29:2899–2916. https://doi.org/10.1007/s10948-016-3587-y

Zeng L, Sun H, Peng T, Zheng W (2019) The sintering kinetics and properties of sintered glass-ceramics from coal fly ash of different particle size. Results Phys 15:102774. https://doi.org/10.1016/j.rinp.2019.102774

Zhang J, Dong W, Li J, Qiao L, Zheng J, Sheng J (2007) Utilization of coal fly ash in the glass–ceramic production. J Hazard Mater 149:523–526. https://doi.org/10.1016/j.jhazmat.2007.07.044

Zhang Z, Zhang L, Li A (2015a) Remedial processing of oil shale fly ash (OSFA) and its value-added conversion into glass–ceramics. Waste Manag 46:316–321. https://doi.org/10.1016/j.wasman.2015.09.007

Zhang Z, Zhang L, Li A (2015b) Development of a sintering process for recycling oil shale fly ash and municipal solid waste incineration bottom ash into glass ceramic composite. Waste Manage 38:185–193. https://doi.org/10.1016/j.wasman.2014.12.028

Zhang D-L, Zhang MY, Zhang CH, Sun YJ, Sun X, Yuan XZ (2016) Pyrolysis treatment of chromite ore processing residue by biomass: cellulose pyrolysis and Cr(VI) reduction behavior. Environ Sci Technol 50:3111–3118. https://doi.org/10.1021/acs.est.5b05707

Zhang S, Zhang Y, Wu T (2018a) Effect of Cr_2O_3 on the crystallization behavior of synthetic diopside and characterization of Cr-doped diopside glass ceramics. Ceram Int 44:10119–10129. https://doi.org/10.1016/j.ceramint.2018.02.231

Zhang H, Du Y, Yang X, Zhang X, Zhao M, Chen H, Ouyang S, Li B (2018b) Influence of rare earth ions on metal ions distribution and corrosion behavior of tailing-derived glass-ceramics. J Non-Cryst Solids 482:105–115. https://doi.org/10.1016/j.jnoncrysol.2017.12.028

Zhang S, Zhang Y, Gao J, Qu Z, Zhang Z (2019a) Effects of Cr_2O_3 and CaF_2 on the structure, crystal growth behavior, and properties of augite-based glass ceramics. J Eur Ceram Soc 39:4283–4291. https://doi.org/10.1016/j.jeurceramsoc.2019.05.060

Zhang Z, Wang J, Liu L, Shen B (2019b) Preparation and characterization of glass-ceramics via co-sintering of coal fly ash and oil shale ash-derived amorphous slag. Ceram Int 45:20058–20065. https://doi.org/10.1016/j.ceramint.2019.06.269

Zhang S, Zhang Y, Qu Z (2020a) Effects of soluble Cr_2O_3 doping on the glass structure, microstructure, crystallization behavior, and properties of MgO–Al_2O_3–SiO_2 sapphirine glass ceramics. Mater Chem Phys 252:123115. https://doi.org/10.1016/j.matchemphys.2020.123115

Zhang Z, Wang J, Liu L, Ma J, Shen B (2020b) Preparation of additive-free glass-ceramics from MSW incineration bottom ash and coal fly ash. Constr Build Mater 254:119345. https://doi.org/10.1016/j.conbuildmat.2020.119345

Zhang P, Muhammad F, Yu L, Xia M, Lin H, Huang X, Jiao B, Shiau Y, Li D (2020c) Self-cementation solidification of heavy metals in lead-zinc smelting slag through alkali-activated materials. Constr Build Mater 249:118756. https://doi.org/10.1016/j.conbuildmat.2020.118756

Zhao M, Cao J, Wang Z, Li G (2019a) Insight into the dual effect of Fe_2O_3 addition on the crystallization of CaO-MgO-Al_2O_3-SiO_2 glass-ceramics. J Non-Cryst Solids 513:144–151. https://doi.org/10.1016/j.jnoncrysol.2019.03.021

Zhao S, Muhammad F, Yu L, Xia M, Huang X, Jiao B, Lu N, Li D (2019b) Solidification/stabilization of municipal solid waste incineration fly ash using uncalcined coal gangue–based alkali-activated cementitious materials. Environ Sci Pollut Res 26:25609–25620. https://doi.org/10.1007/s11356-019-05832-5

Zhao W, Huang X, Yan B, Hu S, Guo H, Chen D (2021) Recycling of blast furnace slag and fluorite tailings into diopside-based glass-ceramics with various nucleating agents' addition. Sustainability 13:11144. https://doi.org/10.3390/su132011144